J. Fluid Mech. (1975), *vol.* 70, *part* 2, *pp.* 393–413
Printed in Great Britain

Mean and fluctuating flow measurements of a fully-developed, non-adiabatic, hypersonic boundary layer

By F. K. OWEN,
United Aircraft Research Laboratories, East Hartford, Connecticut 06108
C. C. HORSTMAN AND M. I. KUSSOY
Ames Research Center, NASA, Moffett Field, California 94035

(Received 23 April 1974)

Extensive boundary-layer measurements have been made on a cone–ogive–cylinder model at a free-stream Mach number of 7·0 and momentum-thickness Reynolds number of 8500. Mean flow transformations and calculated turbulence correlations are presented which are in good agreement with previous incompressible results. New quantitative turbulence measurements including measurements of the first higher moment and probability density of fluctuations in mass flow and total temperature in hypersonic flow are also presented. The higher moment and probability density data show that the characters of the fluctuation modes of the mass flow and total temperature are significantly different in the wall region and in the outer part of the boundary layer. These differences together with data on the turbulence scale and lifetime obtained from autocorrelation and space–time correlation measurements are discussed.

1. Introduction

At present determined efforts are being made to develop methods of predicting turbulent flow behaviour using numerical techniques. However, the rate of development of computational fluid dynamics, especially for compressible flow fields, is no longer dependent on computer size or numerical techniques, but is restricted by the need for improved understanding of both the physics of turbulence and the structure of turbulent flows, which is required to model the turbulent correlations which result from time averaging the Navier–Stokes equations.

Although extensive measurements are available for low speeds, few comprehensive studies of compressible turbulent flow fields have been made, and apart from the work of Laderman & Demetriades (1972) no quantitative turbulence data are available for non-adiabatic flows in the hypersonic regime. Thus little is known about the effects of compressibility and heat transfer on turbulence structure, and interpretation of the effect of these parameters on the few available data is difficult since most measurements have been obtained in nozzle-wall or other non-equilibrium flows where unknown effects of upstream history

must have also been present. Accordingly, further measurements of the structure of the turbulent fluctuations in fully documented compressible flows are essential to obtain more insight into the properties of compressible turbulence. In addition, new turbulence models are now being used in incompressible flow computations which discard the concept of effective turbulent transport properties and employ differential equations for the turbulence fluxes themselves. These equations, which involve higher moments of the turbulent fluctuations, also introduce the concept of turbulence history or 'lifetime', which can only be determined from space–time cross-correlation measurements. Such turbulence properties have never been measured in compressible flows.

With all these previous experimental shortcomings in mind, an experimental programme has been initiated to obtain new turbulence measurements in a fully documented, zero-pressure-gradient, compressible boundary layer on a cone–ogive–cylinder model. In a previous paper (Owen & Horstman 1972) the first hypersonic turbulence structure measurements involving space–time cross-correlations were reported together with a thorough documentation of the mean flow. Distributions of turbulent shear stress and Prandtl number obtained by integration of the time-averaged conservation equations using these measured mean-flow data have also been reported (Horstman & Owen 1972).

In the present paper, further extensive turbulence measurements made using a hot-wire anemometer, including turbulence magnitude, correlation and scale measurements, are reported. We have also made the first measurements of the turbulence lifetime, higher moments and probability density of the fluctuations in the mass flow and total temperature in hypersonic flow. The work has also been extended to study the mean flow in the wall region in much greater detail using improved, miniaturized, total-temperature, Pitot-pressure and static-pressure probes. These new data have been used to calculate the distributions of turbulent shear stress and Prandtl number in the wall region and across the boundary layer.

2. Description of the experiment

2.1. *Wind tunnel*

The investigation was conducted in the Ames 3·5 ft hypersonic wind tunnel, where heated high-pressure air flows through a test section 1·067 m in diameter to low-pressure spheres. The nominal test conditions were: total temperature = 695 °K, total pressure = 34 atm, free-stream unit Reynolds number = $10{\cdot}9 \times 10^6\ \mathrm{m}^{-1}$, free-stream Mach number = 7·0. The test core diameter was approximately 0·7 m with an axial Mach number gradient of less than $0{\cdot}12\ \mathrm{m}^{-1}$.

2.2. *Test model*

The test model was a 10° cone–ogive–cylinder 330 cm long and 20·3 cm in diameter. The cone–ogive section, which was 64·4 cm long, was designed to give zero-pressure-gradient flow over the cylindrical portion. Measured surface-pressure data were in good agreement with characteristics theory although there

was a constant slightly favourable pressure gradient given by

$$p^{-1}\,dp/dx = -4\,\%\ \mathrm{m}^{-1}$$

over the cylinder portion of the model (Owen & Horstman 1972).

Natural transition from laminar to turbulent flow was measured by a hot wire close to the model surface. Using the criteria of Owen (1970) the beginning and end of transition were determined to be at 37 and 80 cm, respectively, from the cone apex.

The present fluctuating and mean flow measurements were obtained at a station 225 cm from the cone apex. Thus the measurements were obtained over 60 average boundary-layer thicknesses downstream of transition in a boundary layer which was self-similar for over 40 average boundary-layer thicknesses upstream of the measurement station. The measured boundary-layer parameters at this station were: edge Mach number $M_e = 6{\cdot}7$, boundary-layer thickness $\delta = 3{\cdot}3$ cm (defined as the height in the boundary layer where the Pitot pressure reaches 99 % of the local free-stream value), momentum thickness $\theta = 0{\cdot}128$ cm, edge Reynolds number $Re_\theta = 8500$, model wall temperature $T_w = 300$ °K.

2.3. *Mean-flow measurements*

In a previous paper (Owen & Horstman 1972) measurements of surface pressure, skin friction and heat transfer from 85 to 237 cm from the cone apex were reported for this model. Assuming constant static pressure through the boundary layer, velocity, density and Mach number profiles were also obtained from Pitot-pressure and total-temperature surveys at 115, 176 and 237 cm from the cone apex. More detailed measurements have now been made (including static-pressure surveys) using new miniaturized probes. Single probes were traversed through the boundary layer, stopping for several seconds at each measurement point to prevent any time lag in the pressure and temperature readings.

Pitot pressure was measured with a rectangular stainless-steel probe (of outside dimensions 0·03 cm high by 0·15 cm wide with a uniform wall thickness of 0·004 cm). Independent calibrations in a free-jet facility, matching the Mach number, velocity and density with the present test conditions, indicated that rarefaction effects were less than 1·0 %. Static-pressure profiles were obtained using a probe geometrically similar (10° cone–cylinder) to those used by Behrens (1963) and Laderman & Demetriades (1972). The probe diameter was 0·10 cm. Independent calibrations to account for viscous interaction effects were in agreement with the calibration data of Behrens (1963). The maximum correction applied to the present data was 7 %. Within the accuracy of the data no static-pressure variation was observed across the present boundary layer. Total-temperature profiles were obtained across an unshielded butt-welded chromel–alumel wire 0·3 cm long and 0·007 cm in diameter with provisions for simultaneous measurement of the support temperature. The probe was similar in design to that used by Vas (1972). Corrections for radiation, conduction and the recovery factor were made following Vas (1972). For the present case the radiation corrections were negligible. Independent calibrations of this probe in the wind-tunnel free stream indicated a maximum total-temperature error of 1·5 %.

2.4. *Hot-wire measurements*

All quantitative turbulence measurements were made with a constant-current anemometer system which had a flat frequency response up to 75 kHz at all wire overheat ratios. Previous attempts to measure the magnitude of the turbulence fluctuations with a constant-temperature anemometer had proved unsuccessful because of the inherent problem of poor frequency response at low overheat ratios (to be discussed in § 2.5).

In compressible flow (Mach number greater than 1·2), the output of the compensated hot-wire anemometer is

$$e' = S_{T_0}\frac{T_0'}{T_0} - S_{\rho u}\frac{(\rho u)'}{\rho u},$$

whose mean-square value is given by

$$\left(\frac{\langle e'\rangle}{S_{T_0}}\right)^2 = \left(\frac{\langle T_0'\rangle}{T_0}\right)^2 - 2\frac{S_{\rho u}}{S_{T_0}}R_{(\rho u)T_0}\frac{\langle(\rho u)'\rangle}{\rho u}\frac{\langle T_0'\rangle}{T_0} + \left(\frac{S_{\rho u}}{S_{T_0}}\right)^2\left(\frac{\langle(\rho u)'\rangle}{\rho u}\right)^2,$$

where $S_{\rho u}$ and S_{T_0} are the usual hot-wire mass-flow and total-temperature sensitivity coefficients defined by Morkovin (1956). Thus, if three fluctuation measurements are made at different wire overheat ratios, three sets of sensitivity coefficients are obtained ($S_{\rho u}/S_{T_0}$ is proportional to the wire overheat ratio) and the resulting set of three independent equations can be solved for the r.m.s. values $\langle T_0'\rangle$ and $\langle(\rho u)'\rangle$ and the correlation $R_{(\rho u)T_0}$ between mass flow and total temperature. However, these three unknowns are usually determined by modal analysis (Kovasznay 1950) and many more overheat values are used to reduce the scatter. In the present experiments, at least ten overheat values were used to construct the mode diagrams. The hot-wire time constants and sensitivity coefficients were determined as outlined by Morkovin (1956) using hot-wire data for the mean flow obtained in the boundary layer and wind-tunnel free stream.

The fluctuations in mass flow and total temperature cannot be decomposed into density, pressure, temperature and velocity fluctuations in compressible flow without additional measurements or assumptions. The information required is the magnitude of the pressure fluctuations and the pressure–velocity, pressure–temperature and pressure–density correlations. So far, data of this type have not been obtained for compressible flow. Consistent with previous compressible data in lower Mach number flows, zero pressure fluctuations were assumed for the decomposition of the present hot-wire signals into velocity and density fluctuations. Kistler (1959) argues that for Mach numbers as high as 4·6 this assumption is reasonable. However, since the pressure fluctuations probably scale with Mach number squared, this assumption may not be valid for the present case. As an alternative to the assumption of zero pressure fluctuations, Laderman & Demetriades (1972) decomposed their data on the modes of mass flow and total temperature into vorticity, entropy and pressure modes, under the assumption that all correlations involving pressure fluctuations are zero and the vorticity–entropy correlation is $-1{\cdot}0$. Comparison of these results with the same data decomposed assuming zero pressure fluctuations indicates

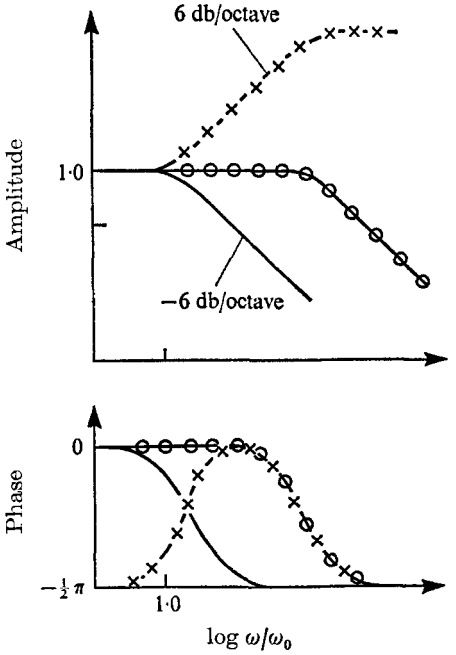

FIGURE 1. Response of constant-current system. ——, uncompensated hot wire; – × – × –, compensating amplifier; –O–O–, combined response.

only small differences in the resulting velocity and density fluctuation data. Thus, although $p' = 0$ is not a strictly valid assumption, it may be adequate to estimate the levels of the fluctuations in velocity and static temperature from the present hot-wire data.

2.5. *Comparison of constant-current anemometer (CCA) and constant-temperature anemometer (CTA) systems*

The fundamental requirement for meaningful quantitative turbulence measurements with a hot-wire anemometer in compressible flows is high-frequency response over a wide range of wire overheat ratios. In an attempt to obtain this requirement, a detailed study of the two anemometer principles was undertaken and showed a significant weakness in the CTA technique. This weakness is illustrated by the following equation for the CTA frequency response:

$$M_{\mathrm{CTA}} = M_{\mathrm{wire}}/(1 + 2rR_w G),$$

where M_{CTA} and M_{wire} are the time constants of the anemometer system and the wire alone, respectively, r is the wire overheat, R_w is the wire resistance and G is the anemometer transconductance. It can be seen that the CTA frequency response is directly proportional to the wire overheat ratio and at low overheat ratios ($r \to 0$) the anemometer-system time constant approaches the wire time constant. Since M_{wire} in the present tests ranged from 1 to 5 ms (frequency response from 32 to 160 Hz), the present low-overheat CTA measurements are clearly open to question.

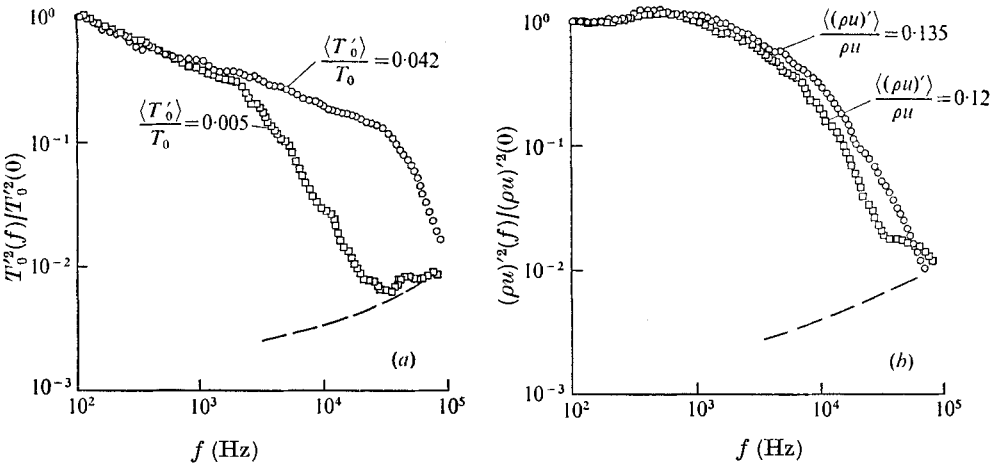

FIGURE 2. Normalized power spectra comparing the constant-current and constant-temperature anemometer systems; $y/\delta = 0{\cdot}23$. ○, constant current; □, constant temperature. (*a*) Low overheats (total-temperature fluctuations). (*b*) High overheats (mass-flow fluctuations).

On the other hand, with the use of compensating amplifiers, adequate CCA response was maintained even at the lowest overheat ratios. The technique of response restoration is shown schematically in figure 1. Consider the uncompensated wire response to turbulent fluctuations, namely a gain of unity until the fluctuation frequency (ω) exceeds the wire roll-off frequency $\omega_0 = M_{\text{wire}}^{-1}$, at which point the response is attenuated at a rate of 6 db/octave with associated phase distortion ($\tan\phi = -\omega/\omega_0$). Thus, if the wire time constant is known, restoration of the signal for frequencies greater than ω_0 can be achieved by means of a phase-matched 6 db/octave amplifier as shown in figure 1. Although the wire time constant is a function of both the overheat and local flow variables, it can be calculated from the characteristics of the wire material and the measured mean wire resistance and current (Morkovin 1956). The amplifier gain frequency can then be matched to the wire roll-off frequency during the experiment. In our subsequent data reduction programme any slight mismatch during the experiment was accounted for in the calculations using the measured fluctuating wire voltage. Ultimately the compensated wire response is governed by the upper frequency limit of the amplifier and the lowest wire time constants encountered in the experiment. Although amplitude restoration can be achieved to a higher frequency than phase restoration, the mean-square signal is still correct up to the amplitude compensation limit, which in the present work was 75 kHz at the lowest wire overheats.

To illustrate the problems encountered with the CTA system, the two anemometers were used to obtain fluctuation data for a wide range of overheat ratios at the same position in the boundary layer ($y/\delta = 0{\cdot}23$). The normalized power spectra are compared in figure 2 and the modal analyses for the two systems are compared in figure 3. The data in figure 2(*a*) are for low wire overheat ratios (corresponding to total-temperature fluctuations) while figure 2(*b*) shows

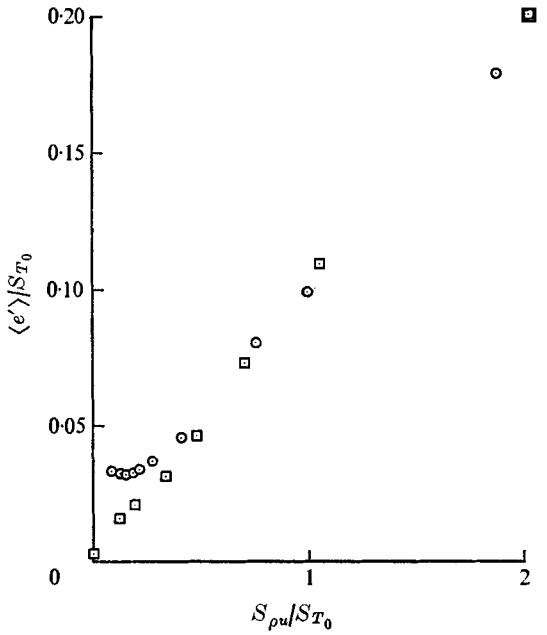

FIGURE 3. Modal analysis comparing the constant-current and constant-temperature anemometer systems; $y/\delta = 0{\cdot}23$. ○, constant current; □, constant temperature.

data for high wire overheats (corresponding to mass-flow fluctuations). It is seen that the frequency response of the CTA system is inadequate at the low overheats while the two systems agree well at high overheat ratios. The r.m.s. fluctuation levels obtained from the modal analyses are also shown in figure 2. Although the mass-flow fluctuation levels obtained by the two systems are in good agreement, the CTA total-temperature data (obtained from the intercept of the data at zero mass-flow sensitivity in figure 3) are significantly reduced because of the low frequency response of the system at low overheat ratios. In addition, the correlation $R_{(\rho u)T_0}$ is obtained primarily from low-overheat data; thus, in the present experiments (figure 3), the CTA system is clearly inadequate for accurate measurements of both total-temperature fluctuations and correlations between mass flow and total temperature. For this reason, all quantitative turbulence measurements in these tests were made with a CCA system.

3. Measurements of mean flow field

Measurements of mean velocity, Mach number and density are presented in figure 4. For this compressible non-adiabatic boundary layer, the boundary-layer edge defined by the velocity profile ($U/U_e = 0{\cdot}995$) is located at $y/\theta = 22$ and does not include the entire 'density' boundary layer. For the present experiment the boundary-layer edge $y = \delta$ is defined as the height in the boundary layer where the measured Pitot pressure reaches 99 % of the local free-stream value ($y/\theta = 25{\cdot}8$). The experimental temperature–velocity relationship for these data is shown in figure 5; also shown are the linear (Crocco) and quadratic

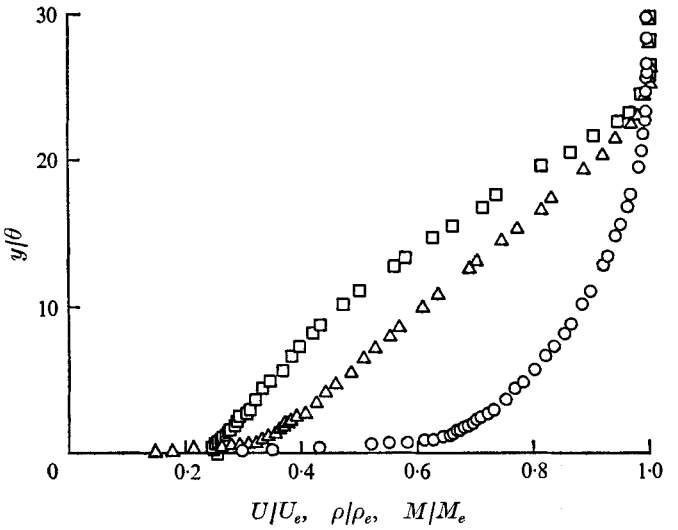

FIGURE 4. Mean measurements across the boundary layer. ○, U/U_e; □, ρ/ρ_e; △, M/M_e.

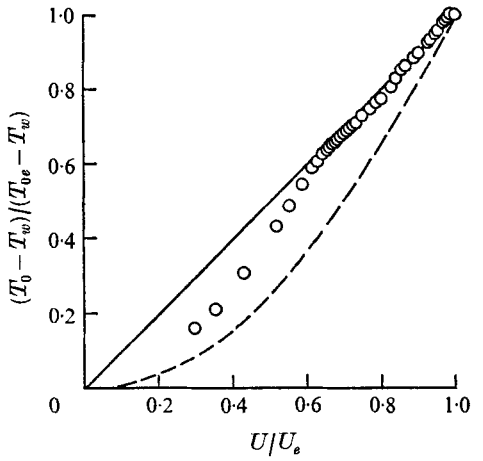

FIGURE 5. Relation between velocity and total-temperature distribution across the boundary layer. ——, linear; – – –, quadratic.

relationships. Except in the region close to the wall the data are approximated by the linear relationship. This is in contrast to previous non-equilibrium data (e.g. Laderman & Demitriades 1972), which follow the quadratic relationship through most of the boundary layer.

Important methods used to predict compressible turbulent boundary-layer flow fields are compressible–incompressible transformation techniques. Several transformation techniques have been previously evaluated for this flow (Owen & Horstman 1972). It was concluded that the Van Driest (1951) transformation was superior to the other methods. The present data have been transformed to incompressible law-of-the-wall co-ordinates (figure 6*a*) and velocity-defect co-ordinates (figure 6*b*) using the Van Driest transformation with a wall friction

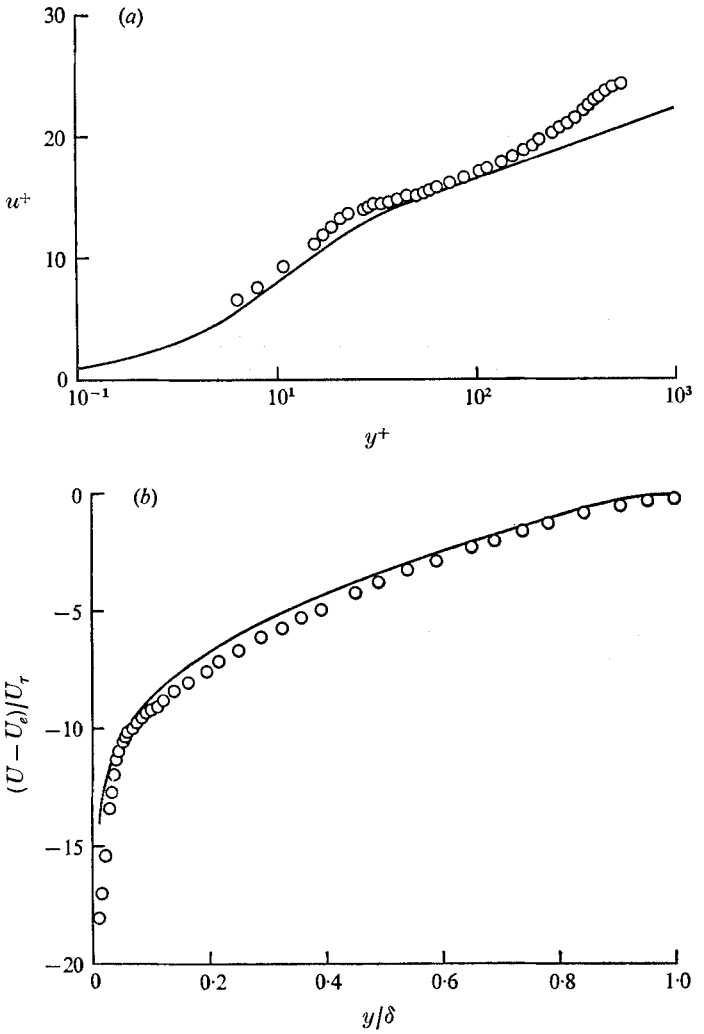

FIGURE 6. (*a*) Law-of-the-wall correlation and (*b*) velocity-defect profile in incompressible co-ordinates using the Van Driest transformation. ——, incompressible correlation, Coles (1953).

velocity determined from direct skin-friction measurements. A comparison with the incompressible correlation curve of Coles (1953) indicates the adequacy of the transformation. Near the wall (figure 6*a*) the data are in good agreement with the incompressible law-of-the-wall correlation with the sublayer data ($y^+ < 15$), closely approaching the linear relationship $u^+ = y^+$. In the outer or wake portion of the boundary layer (figure 6*b*) the data are in good agreement with the incompressible velocity-defect correlation.

Having previously shown the similarity of the profiles along the model, the present data have been integrated across the boundary layer to determine the turbulent shear stress and heat flux following the analysis of Horstman & Owen (1972). The distributions of the Prandtl mixing length l, eddy viscosity ϵ and

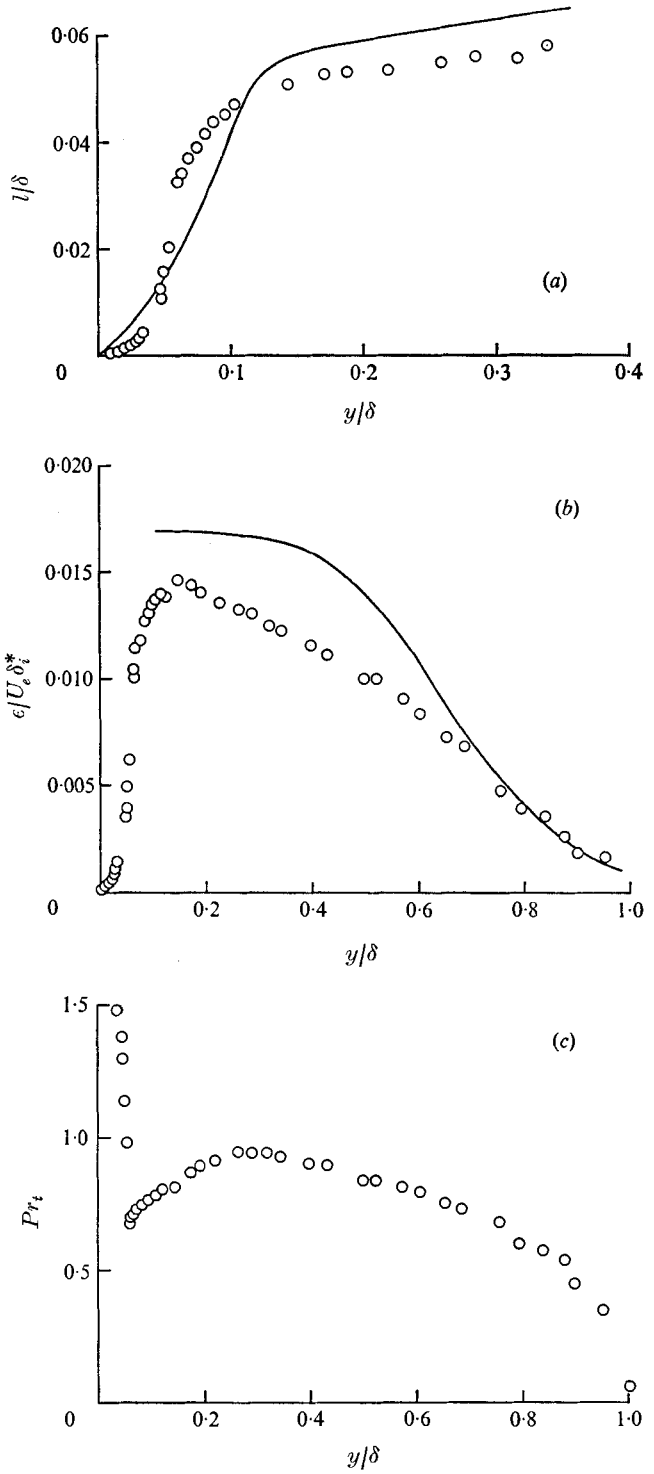

FIGURE 7. Distributions of (*a*) mixing length, (*b*) eddy viscosity and (*c*) turbulent Prandtl number across the boundary layer. ——, turbulence model, Cebeci (1971).

turbulent Prandtl number Pr_t across the boundary layer were evaluated using these results for the shear stress and heat flux. These distributions are shown in figures 7(*a*), (*b*) and (*c*) respectively. Also, a representative model for the turbulent flow properties proposed by Cebeci (1971) is compared with the normalized mixing-length and eddy-viscosity distributions. Near the wall (figure 7*a*) the data are in only fair agreement with the model. However, it should be pointed out that for $y/\delta < 0{\cdot}05$ the assumption of boundary-layer similarity is probably invalid, which casts doubts on the accuracy of the mixing-length data in this region. For the outer portion of the boundary layer (figure 7*b*) the eddy-viscosity model overpredicts the data by as much as 30%. But considering that this model is based on incompressible flow measurements this small disagreement between the model and the present data is very satisfactory.

The results for the turbulent Prandtl number (figure 7*c*) vary across the entire boundary layer and near the wall indicate a Prandtl number greater than unity. These results are in excellent qualitative and quantitative agreement with the adiabatic results of Meier & Rotta (1971).

4. Turbulence measurements

The mass-flow and total-temperature measurements through the boundary layer are compared in figures 8(*a*) and (*b*) with previous adiabatic compressible measurements of Kistler (1959) and with the only available non-adiabatic results, of Laderman & Demetriades (1972). Although Kistler found that the intensities of both fluctuation modes increased with Mach number, the mass-flow fluctuations do appear to be independent of Mach number above $M = 5{\cdot}0$ while the total-temperature fluctuations appear to decrease with increasing Mach number in the non-adiabatic hypersonic regime. This implies that the effect of heat transfer is to reduce the total-temperature fluctuations.

Measurements of the correlation between mass flow and total temperature are shown in figure 8(*c*). These data also show that the hypersonic results do not follow the trend set by Kistler's adiabatic compressible data and are significantly different over the outer half of the boundary layer.

The present correlation-coefficient data for the local free stream ($y/\delta = 1{\cdot}1$) agree with previous unpublished results obtained by the authors in the wind-tunnel free stream, where $R_{(\rho u)\,T_0} = -0{\cdot}7$. Again, this points to differences between adiabatic and non-adiabatic compressible flows. Previous adiabatic measurements of Laufer (1961) and, indeed, the unheated hypersonic measurements of Wagner, Madalon & Weinstein (1970) indicate that, in the free stream, the sound field dominates the other modes (i.e. $R_{(\rho u)\,T_0} = -1{\cdot}0$). The present non-adiabatic results show that several modes coexist in both the local and undisturbed free stream (i.e. $R_{(\rho u)\,T_0} \neq -1{\cdot}0$). However, this is to be expected since temperature fluctuations produced by the heater will be present in the test section and thus will give rise to a different correlation function in the free stream.

Assuming zero pressure fluctuations, the hot-wire signals are interpreted in terms of velocity and density fluctuations in figures 9, 10 and 11. These results

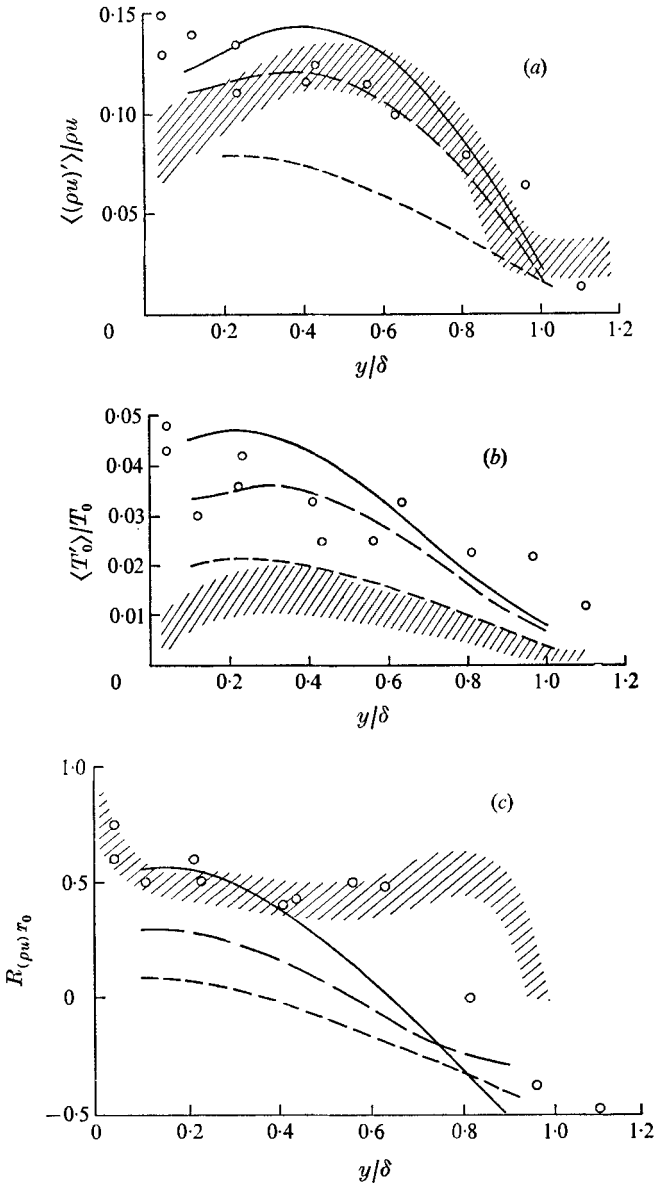

FIGURE 8. Distributions of (*a*) mass-flow fluctuations, (*b*) total-temperature fluctuations and (*c*) correlation between mass flow and total temperature across the boundary layer. ○, present data, $M_e = 6{\cdot}7$, $T_w/T_0 = 0{\cdot}46$; ——, Kistler (1959), $M_e = 4{\cdot}67$, $T_w/T_0 = 1{\cdot}0$; — —, Kistler (1959), $M_e = 3{\cdot}56$, $T_w/T_0 = 1{\cdot}0$; – – –, Kistler (1959), $M_e = 1{\cdot}72$, $T_w/T_0 = 1{\cdot}0$; /////, Laderman & Demetriades (1972), $M_e = 9{\cdot}4$, $T_w/T_0 = 0{\cdot}38$.

are compared with previous compressible data (also decomposed assuming zero pressure fluctuations) and with the incompressible zero-pressure-gradient results of Klebanoff (1954). (The key to previous data is given in figure 8.) The present velocity fluctuations normalized by the wall friction velocity (calculated using a direct measurement of wall shear) shown in figure 9 agree very well with the

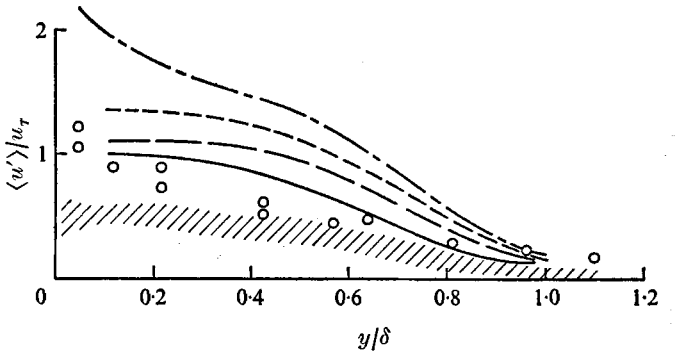

FIGURE 9. Distribution of the normalized velocity fluctuations across the boundary layer. —·—, Klebanoff (1954). (Other notation as in figure 8.)

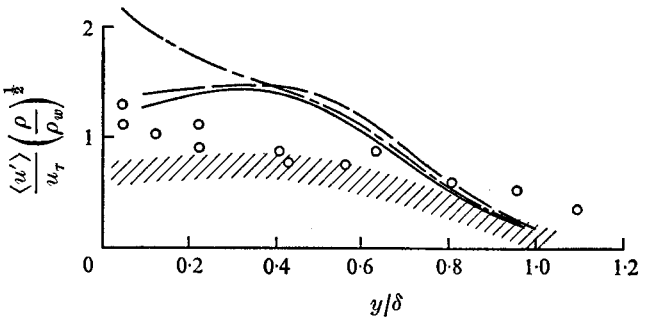

FIGURE 10. A test of Morkovin's co-ordinate stretching density factor applied to the velocity fluctuations. (Notation as in figure 8.)

Mach number trend set by previous incompressible and compressible results. However, if Morkovin's co-ordinate stretching density factor (Morkovin 1961) is applied (figure 10), neither set of high Mach number data collapses onto the Klebanoff–Kistler curve. Figure 11 shows another instance where hypersonic measurements do not follow the trend set by lower Mach number results, since the density fluctuations seem to be independent of Mach number above $M \approx 5{\cdot}0$.

Since the validity of Taylor's hypothesis in this shear flow has already been demonstrated, it is possible to make the transformation $d/dx = U_c^{-1} d/dt$ and to determine the microscales and integral scales of the modal fluctuations from autocorrelation measurements. If one defines these scales according to Hinze (1959, p. 37) the results (figure 12) show that the mass-flow scales are somewhat larger than the total-temperature scales across the entire boundary layer. The spectra found using a constant-current anemometer also show scale differences between the two fluctuation modes. From the shapes of the spectra in figures 2(*a*) and (*b*), the total-temperature fluctuations clearly contain relatively more high frequency (small scale) energy than the mass-flow fluctuations. If these spectra are normalized by their respective calculated integral length scales, the mass-flow spectra agree with those of Kovasznay (1950) whereas the total-temperature spectra do not. These differences in scale suggest that the characters of the fluctuation modes may well be different, as is indeed the case.

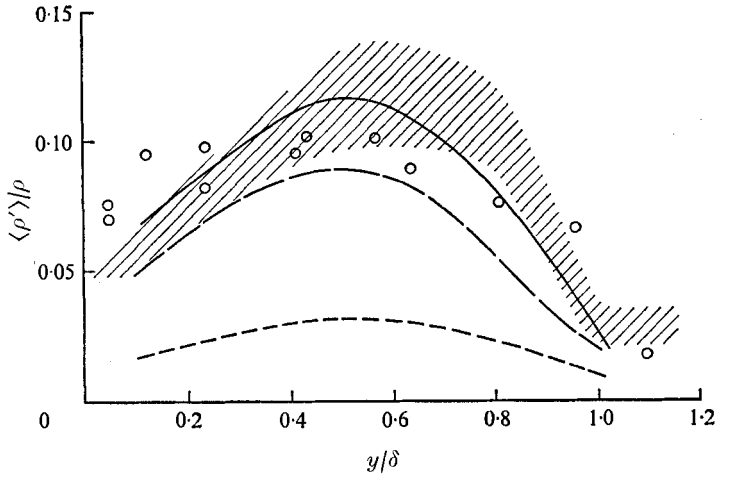

FIGURE 11. Distribution of the density fluctuations across the boundary layer. (Notation as in figure 8.)

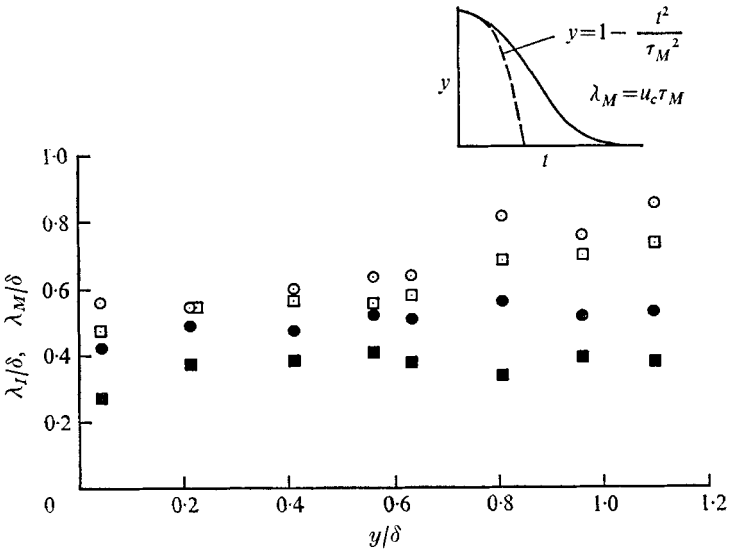

FIGURE 12. Distribution of normalized integral scales λ_I and microscales λ_M of the mass-flow and total-temperature fluctuations across the boundary layer. ○, λ_I, mass flow; ●, λ_M, mass flow; □, λ_I, total temperature; ■, λ_M, total temperature.

Probability density distributions of the mass-flow and total-temperature fluctuations obtained across the entire boundary layer illustrate some of these differences. In the wall region ($y^+ \approx 15$), the mass-flow and total-temperature fluctuations are both non-Gaussian and highly skewed (figure 13*a*). However, since the dimensionless mean-flow gradients in this region are similar, the extent of the deviations from the mean reflects the differences in scale between the two modes. The fact that both modes are negatively skewed suggests that the predominant fluctuations originate near the wall (a region of lower mean mass flow

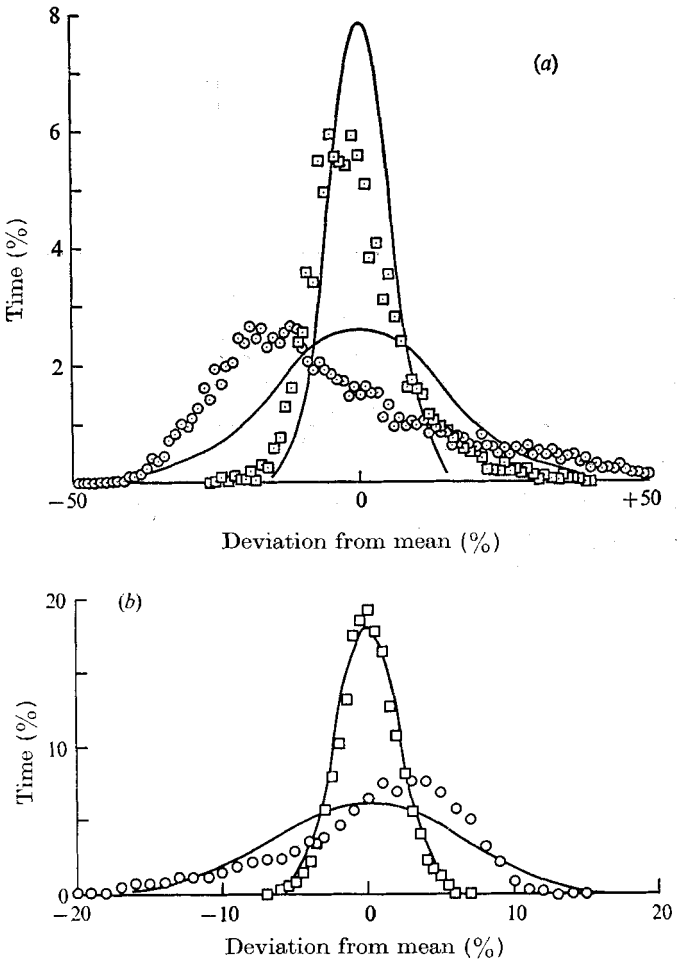

FIGURE 13. Probability density distributions of the mass-flow and total-temperature fluctuations. ○, mass flow; □, total temperature; ——, Gaussian. (*a*) $y/\delta = 0{\cdot}04$. (*b*) $y/\delta = 0{\cdot}96$.

and total temperature), which agrees with our previous correlation measurements, which implied the trajectories of the turbulent fluctuations.

At the outer edges of the boundary layer (figure 13*b*), the mass-flow skewness is reversed, indicating entrainment of higher mass flow from the local free stream. The percentage deviations are much reduced in comparison with the data near the wall since they scale with the smaller mean-flow gradients in the outer region. On the other hand, the total-temperature fluctuations are practically Gaussian since here the total-temperature profile is flat and the fluctuations, like those in the free stream, probably result from upstream conditions and are not a result of local mixing.

Composite plots of the probability density distributions across the boundary layer are shown in figures 14 (*a*) and (*b*). Over the central portion of the boundary layer, both fluctuation modes are Gaussian, although again the amplitudes of

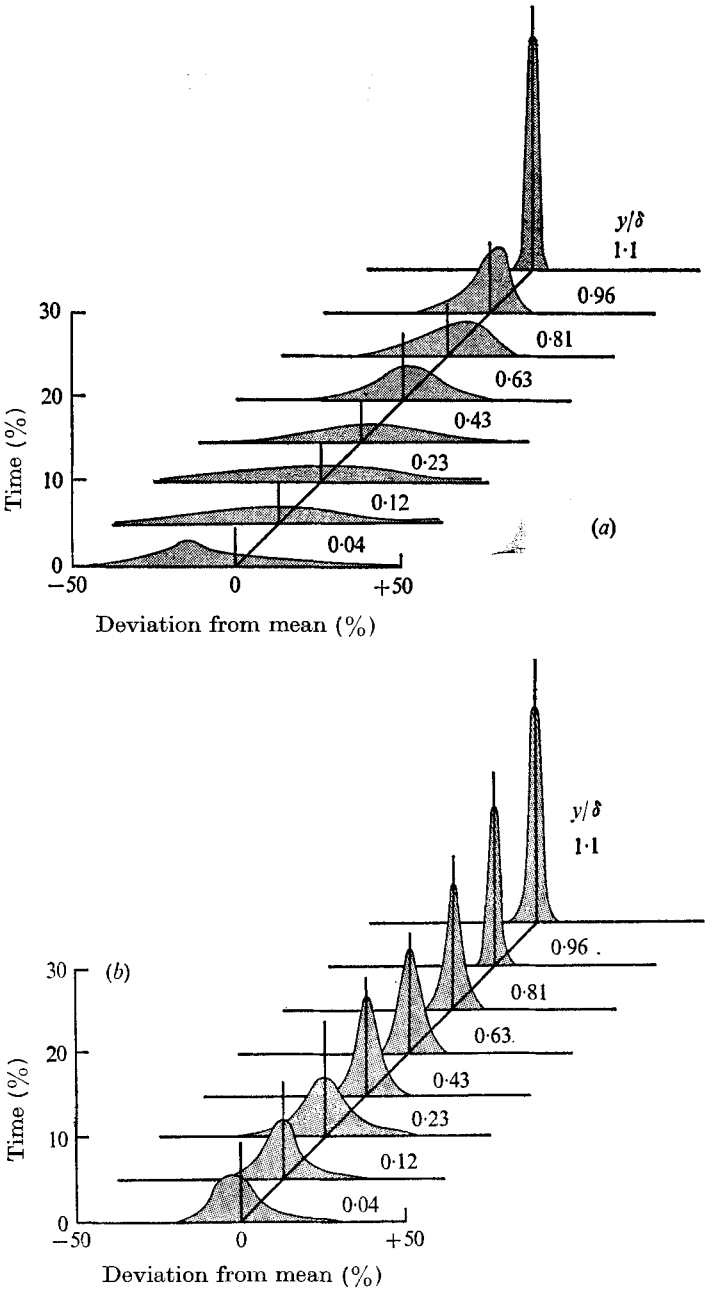

FIGURE 14. A composite sketch of the probability density distributions of the fluctuating quantities across the boundary layer. (*a*) Mass flow. (*b*) Total temperature.

the mass-flow fluctuations are much greater, reflecting the differences in the fluctuation scales of the two modes.

The dimensionless third (skewness) and fourth (flatness) moments of the mass-flow and total-temperature fluctuations are shown in figures 15(*a*) and (*b*). These data show that, as expected from the shapes of the probability densities,

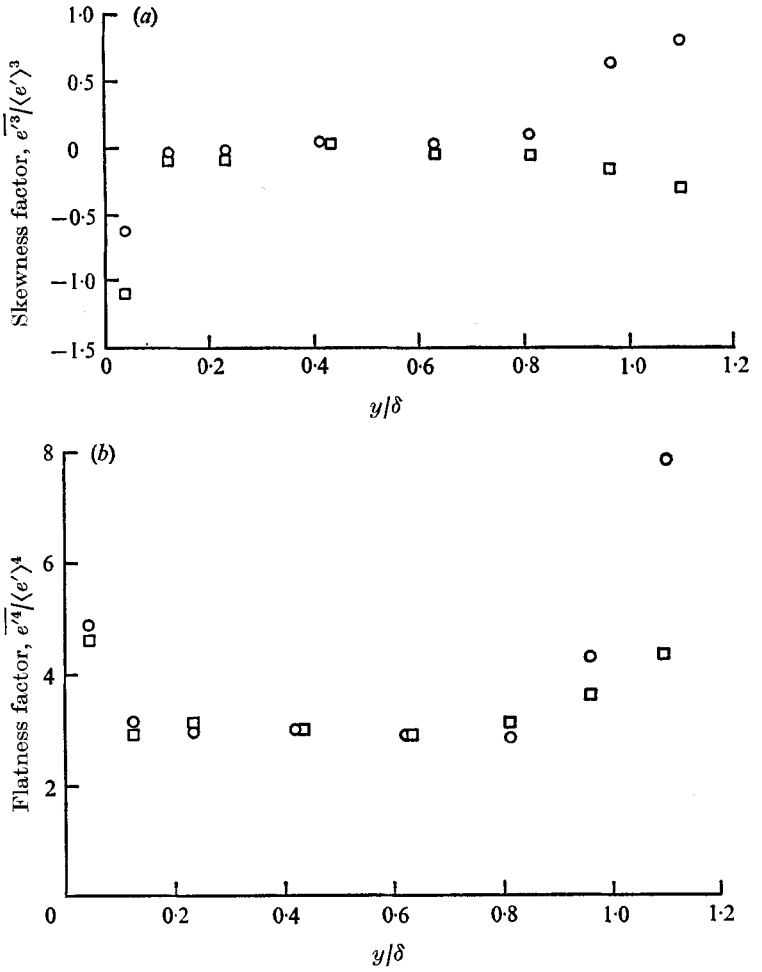

FIGURE 15. Distributions of (*a*) the third moment (skewness) and (*b*) the fourth moment (flatness) of the mass-flow and total-temperature fluctuations across the boundary layer. ○, mass flow; □, total temperature.

the skewness and flatness are zero and three, respectively, over the central portion of the boundary layer. In the viscous sublayer ($y/\delta < 0{\cdot}05$), however, the skewness reaches a negative value in excess of unity and strong intermittency is suggested by flatness factors approaching 5·0. In the outer regions of the boundary layer, similar deviations of the flatness factors from their nominal Gaussian value of 3·0 are observed, and the values of the skewness of the mass-flow fluctuations are of opposite sign from the sublayer data.

Intermittency distributions across the boundary layer were calculated using the flatness-factor data and are shown in figure 16. Significant differences between these results and the data of Klebanoff are apparent. Owing to the increased thickness of the viscous sublayer at hypersonic speeds, wall-region intermittency was detected and is clearly evident in the hot-wire traces (see appendix). In the outer flow, the onset of intermittency is more sharply defined but does not occur

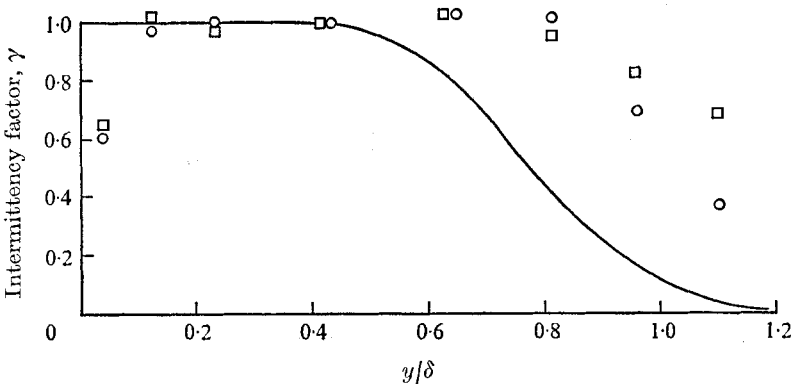

FIGURE 16. Intermittency distribution across the boundary layer. ○, mass flow; □, total temperature; ——, Klebanoff (1954), velocity.

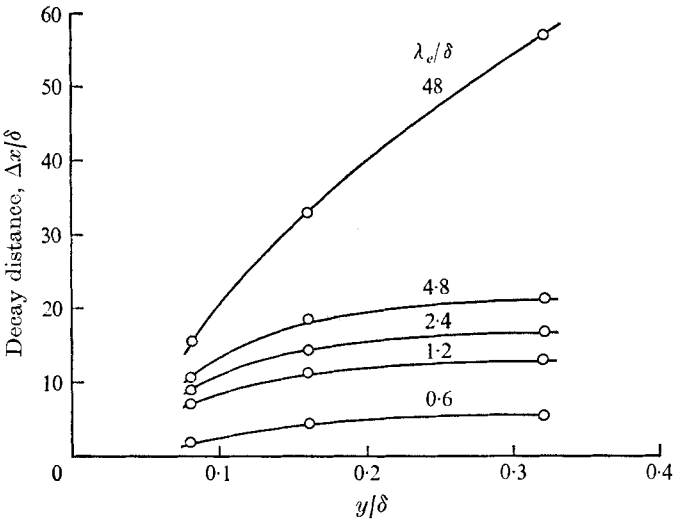

FIGURE 17. Turbulence lifetime distributions for various turbulent scales of the mass-flow fluctuations across the boundary layer. $\lambda_e = U_e/2\pi f$.

until y/δ is much larger than in the low-speed case. Perhaps the present intermittency distribution could be related to the measured $R_{(\rho u)T_0}$ distribution shown in figure 8(*c*).

The qualitative space–time correlation measurements of Owen & Horstman (1972) have been used to estimate the 'lifetimes' of the fluctuations as they are swept along by the mean flow. Although the idea of a 'turbulence lifetime' should not be taken too literally, the measured optimum space–time correlations were assumed to decay exponentially and the appropriate time constants determined from these curves. Previously measured disturbance convection velocities were used to calculate the 'decay constants' for the filtered turbulent field. The results for various turbulent scales are shown in figure 17, where $\lambda_e/\delta \approx 0{\cdot}6$ is representative of the total turbulent field. It is evident that these decay constants are

strong functions of both scale and local mean-flow gradients (i.e. y/δ). Since the duration of any phenomenon is approximately three times its time constant, it is also evident that large eddies persist for extremely long distances (i.e. many boundary-layer thicknesses).

5. Concluding remarks

Detailed mean-flow measurements have shown that, when Van Driest (1951) variables are used, the equilibrium hypersonic boundary-layer law-of-the-wall and velocity-defect profiles are in excellent agreement with Coles' (1953) incompressible correlations. Calculated distributions of turbulent shear stress and Prandtl number are also in very satisfactory agreement with previous incompressible results.

However, it is important to note that the Van Driest formulation assumes constant static pressure and a linear (Crocco) temperature distribution across the boundary layer. Although both conditions were met in this experiment, this is not normally the case for flows in which significant effects of upstream history are present. Thus these results, which are in such strong contrast with many previous non-equilibrium flow measurements, emphasize the need to distinguish between true high Mach number effects and the effects of unknown upstream influence.

Perhaps the most significant result of the quantitative turbulence measurements is that large differences were detected between the mass-flow and total-temperature fluctuation modes. Not only were the scales different, but the probability density and skewness were significantly different across most of the boundary layer. Such differences, especially in the wall region, could well be responsible for the overshoot in the turbulent Prandtl number calculated in this region.

Finally, the long turbulence lifetimes which can be inferred from space–time correlation measurements illustrate a major objection to turbulence models based on local flow conditions. It cannot be assumed that turbulence is uniquely related to local conditions, and flow history must be considered, especially when attempting to calculate non-equilibrium flows.

This work was carried out at N.A.S.A. Ames Research Center when the senior author was the principal investigator on N.A.S.A. Grant no. 05-017-029.

Appendix

At high overheat ratios, the hot wire responds primarily to mass-flow fluctuations, so that, for the constant-current anemometer, periods of mass-flow defect are associated with positive voltage fluctuations, i.e. positive spikes on the a.c. coupled oscilloscope traces. At low overheat ratios, the hot wire responds primarily to total-temperature fluctuations and the situation is reversed, i.e. positive spikes correspond to periods of increased total temperature. Hot-wire oscilloscope traces of the two modal fluctuations are shown in figure 18.

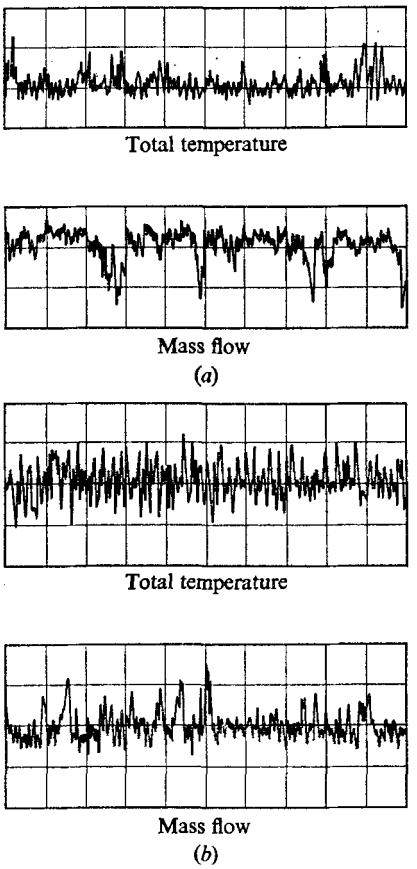

FIGURE 18. Oscilloscope traces of the mass-flow and total-temperature fluctuations (0·2 ms per division). (*a*) $y/\delta = 0{\cdot}04$. (*b*) $y/\delta = 0{\cdot}96$.

In the wall region, the flow is predominantly turbulent with frequent bursts of fluid with lower mass flow and total temperature which must have originated near the wall. In the outer flow, the mass-flow trace is reversed, which indicates entrainment of fluid with higher mass flow from the free stream, whereas the total-temperature fluctuations are symmetrical.

REFERENCES

BEHRENS, W. 1963 *A.I.A.A. J.* **1**, 2864.
CEBECI, T. 1971 *A.I.A.A. J.* **9**, 1091.
COLES, D. 1953 *Jet Propulsion Lab., California Inst. Tech. Rep.* no. 20–69.
HINZE, J. O. 1959 *Turbulence.* McGraw-Hill.
HORSTMAN, C. C. & OWEN, F. K. 1972 *A.I.A.A. J.* **10**, 1418.
KISTLER, A. L. 1959 *Phys. Fluids*, **2**, 290.
KLEBANOFF, P. S. 1954 *N.A.C.A. Rep.* no. 1247.
KOVASZNAY, L. S. G. 1950 *J. Aero. Sci.* **17**, 565.
LADERMAN, A. J. & DEMETRIADES, A. 1972 *Philco Ford Corp. Publ.* U-5079.
LAUFER, J. 1961 *J. Aero Sci.* **28**, 685.

MEIER, H. U. & ROTTA, J. C. 1971 *A.I.A.A. J.* **9**, 2149.
MORKOVIN, M. V. 1956 *AGARDograph*, no. 24.
MORKOVIN, M. V. 1961 *Mécanique de la Turbulence, Colloq. Int. C.N.R.S.* no. 108.
OWEN, F. K. 1970 *A.I.A.A. J.* **8**, 518.
OWEN, F. K. & HORSTMAN, C. C. 1972 *J. Fluid Mech.* **53**, 611.
VAN DRIEST, E. R. 1951 *J. Aero. Sci.* **18**, 145.
VAS, I. E. 1972 *A.I.A.A. J.* **10**, 317.
WAGNER, R. D., MADALON, D. V. & WEINSTEIN, L. M. 1970 *A.I.A.A. J.* **8**, 1964.